XX IMEKO World Congress
Metrology for Green Growth
September 9–14, 2012, Busan, Republic of Korea

SYSTEM FOR AUTOMATIC CHARACTERIZATION OF GIANT MAGNETO-IMPEDANCE SAMPLES

J. H. C. C. Carneiro, E. Costa Silva, L. A. P. Gusmão, C. R. H. Barbosa and E. Costa Monteiro

PUC-Rio, Rio de Janeiro, Brazil, edusilva@ele.puc-rio.br

Abstract: This paper describes an automatic characterization system designed for the measurement of the electric impedance of Giant Magneto-Impedance (GMI) samples. The high speed of measurement attained with the use of this system, designed in the LabVIEW development environment, allows for the rapid determination of the optimal operational point of an eventual GMI magnetometer.

Keywords: GMI, Giant Magneto-Impedance, Automatic Characterization System, Impedance Measurements, Magnetic Sensors.

1. INTRODUCTION

The successful use of Giant Magneto-Resistive (GMR) materials in the construction of precision magnetometers in the field of spintronics, in conjunction with the recent concession of the 2007 Nobel Prize in Physics to GMR's coinventors, Albert Fert and Peter Grünberg, has spurred much activity by research groups in the GMI effect.

Although similarly named, the GMR and GMI effects differ in their nature. While GMR has explanations in quantum mechanics, GMI is derived from the skin effect [1].

The GMI effect is a physical phenomenon characterized by large variations in the electrical impedance when soft amorphous ferromagnetic samples of specific composition are subjected to an external magnetic field. Research in the effect has shown that, with further sophistications, magnetometers based on GMI technology may have enough resolution to replace even SQUIDs (Superconducting Quantum Interference Devices), the currently most sensitive magnetometers, essential for some critical applications [2-8]. In the area of biomagnetism, an eventual GMI magnetometer has promising potential uses, because of the speculated resolution around the order of some picoteslas [3-4, 8].

Examples of biomedical applications that use GMI technology are a pressure transducer used for the non-invasive measurement of arterial pulse waves [5] and a magnetic transducer aimed at the detection of magnetic foreign bodies inserted in the human body [6], both developed in the Laboratory of Biometrology (LaBioMet) at PUC-Rio.

In effect, nowadays, there is no accurate mathematical model for the impact of the various physical parameters that influence the GMI effect. Among that set of parameters, it can be mentioned: geometry of the sample, temperature of the measuring environment, frequency of the biasing current, etc. However, the GMI samples can be electrically modeled by a simple RL model of a resistor in series with an inductor. Further sophistications in this simplistic model are only possible after an analysis of experimental data.

In the research carried out by the LaBioMet personnel, aiming at defining the set of parameters that optimizes the sensitivity of the GMI sensor elements, the impact of various parameters is estimated via multiple experimental measurements [7]. The large number of variables that should be analyzed in the measuring procedure constitutes a motivation for the development of an automatic characterization system which accepts as input a list of measuring configurations, and exports as output the resulting measurement data – readings of magnitude and phase of the impedance of GMI samples.

2. GIANT MAGNETO-IMPEDANCE

The GMI parameter, as defined by many authors [9-10], is based on the percent variation of the impedance magnitude of the sample:

$$GMI(H) \stackrel{\text{def}}{=} \left[\frac{|Z(H)| - |Z(H_{MAX})|}{|Z(H_{MAX})|}\right] \cdot 100 \quad (1)$$

where H_{MAX} indicates the maximum magnetic field that is part of the measurement domain. This magnetic field value is generally defined as the point where the GMI effect has saturated. In other words, the GMI parameter measures the variation of the sample impedance in relation to the applied external magnetic field. However, focusing on the amplification of the absolute impedance values, the following alternative definition has been used:

$$GMI(H) \stackrel{\text{def}}{=} Z(H) - Z(H_O) \quad (2)$$

where H_O indicates the condition where the magnetic field is null ($H_O = 0\ Am^{-1}$). This concept expands into two further and useful definitions, the GMI based on the magnitude (3) and phase (4) characteristics,

$$GMI_{|Z|}(H) \stackrel{\text{def}}{=} |Z(H)| - |Z(H_O)| \quad (3)$$

$$GMI_{\theta[Z]}(H) \stackrel{\text{def}}{=} \theta[Z(H)] - \theta[Z(H_O)] \quad (4)$$

where the GMI is defined as a function of the sample impedance at the origin, i.e. at the point where the magnetic field is null $H_O = 0\ Am^{-1}$. Note that the parameters may assume negative values.

Equations (1) to (4) require the measurement of the impedance of the GMI sample. Figure 1 demonstrates that this information can be acquired via conventional impedance measurements. A current source with a known waveform evokes a voltage drop across the GMI sample, which is measured using an adequate device [4-12].

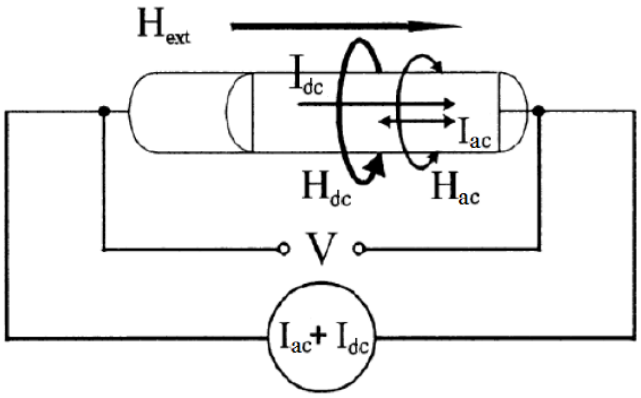

Figure 1: Configuration for the measurement of the impedance of the GMI sample, obtained by means of the voltage drop divided by the applied current.

Figure 1, besides other details, shows that the amorphous ferromagnetic material exhibits an internal and circumferential magnetic field that certainly affects the sample impedance [10]. As mentioned in the introduction, there is a wide variety of external factors that can impact the GMI effect on a sample. For example, the frequency of the current that flows through the sample, I_{ac}, directly modifies the skin effect and therefore the GMI behavior. Also, the DC current, I_{dc}, is responsible by AGMI (Asymmetric Giant Magneto-Impedance) effects [11-12], while small changes in the chemical composition of the sample material can often have dramatic effects on GMI percentages [12].

Other parameters that directly impact the GMI effect are sample temperature, geometric dimensions of the material, AC current, manufacturing process, magnetostriction, applied pressure and many more [9]. As in most materials that are influenced by magnetic phenomena, GMI samples suffer from magnetic hysteresis [9], which certainly accounts as an obstacle for the construction of a magnetometer, and consequently should be carefully analyzed.

3. DESCRIPTION OF THE SYSTEM

With the objective of analyzing each parameter's contribution individually, a controlled measuring environment was constructed for the system. As seen in Fig. 2, the developed system is composed of six parts essential to its functionality: a Helmholtz coil for the generation of the external magnetic field; an LCR meter that electrically excites the sample and, simultaneously, measures its impedance; a current source (I_H) to excite the Helmholtz coil; a polarity inverter to change the direction of the current source; digital controls via a DAQ (Data Acquisition Device) module outputs to control the polarity inverter; and, finally, the software developed in LabVIEW to serve as a virtual interface between the operator and the other modules. In addition, the Helmholtz coil current range is normally fixed, while other electrical parameters are variable, once at a time, if and only if all others are kept constant. In this way, the contribution of each parameter can be isolated for posterior analysis.

The variation of the magnetic field, in Am^{-1}, generated by the Helmholtz coil was controlled by a DC current source according to

$$H = \frac{8NI_H}{5\sqrt{5}R} \quad , \qquad (5)$$

where H is the magnetic field in the center of the Helmholtz coil, N the number of turns, I_H the current that flows through the coils and R the radius of the coils.

The Helmholtz coils have 48 turns and a radius of 15 cm, yielding

$$H[Am^{-1}] = 228.97 \times I_H[A]. \qquad (6)$$

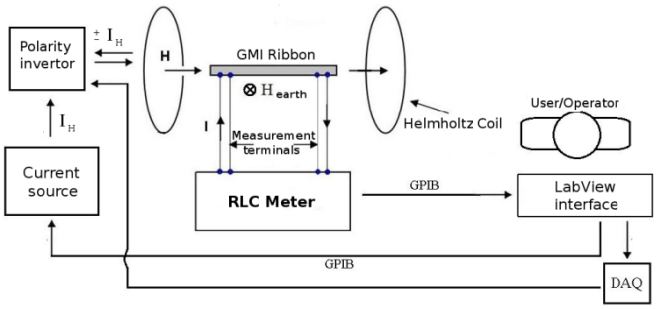

Figure 2: Basic setup of the automatic system for GMI sample characterization.

The system was tested with ribbon-shaped samples having a chemical composition of $Co_{70}Fe_5Si_{15}B_{10}$ due to its extremely low magnetostriction [11], which is a property of ferromagnetic materials that causes them to vary in shape with magnetization. This ribbon property allows for the assumption that the sample's physical geometry is kept constant.

The studied samples are of the LMI (Longitudinal Magneto-Impedance) type, and then it is recommended that, during the measurement process, the GMI ribbon be positioned in a way that the Earth's magnetic field is perpendicular to its length [5-7, 10, 12]. In this way, noise caused by the Earth's magnetic field is minimized. Notice on Fig. 2 that the GMI ribbon and the coils are illustrated in an upright view, emphasizing the need to position them according to the direction of the Earth's magnetic field.

As indicated by Fig. 2, the LCR meter is connected directly to the terminals of the GMI ribbon. To obtain an impedance reading, as needed by equations (3) and (4), the LCR acts as a source of sinusoidal current and measures the voltage drop across the sample. The impedance is simply a relationship between the output voltage and the input current: *Z(jw) = V(jw)/I(jw)*.

The selection of the experimental configurations, in the software developed in LabVIEW, is made by the user. Specifically, the user creates, via a simple graphical interface, a list of experiments to carry out.

The output of the software is raw measurement data, in the form of various Microsoft Excel spreadsheet files that are saved automatically with standardized names to the host computer. These files contain $|Z|$ and θ (magnitude and phase characteristics of the impedance) values and calculated R and L (resistance and inductance) values with corresponding H (Helmholtz coil controlled magnetic field) independent values. Also, the files include graphs with hysteresis characteristics and respective averaged values. For instance, consider the following experiment: a GMI sample of $Co_{70}Fe_5Si_{15}B_{10}$ alloy is subjected to a measurement temperature of 298K, bias current of 80 mA, excitation current of 10 mA and 240 kHz of frequency, to obtain the hysteresis graph indicated by Fig. 3. The linear region of the impedance characteristics is the one indicated for a magnetometer implementation.

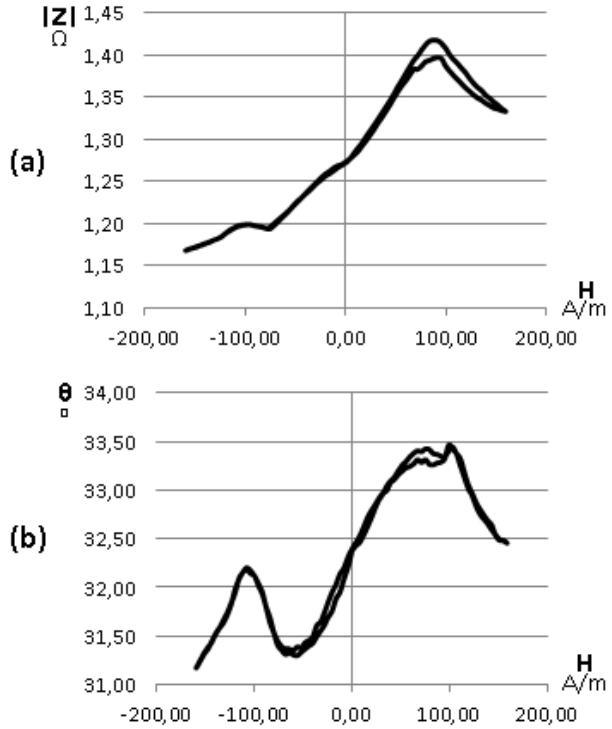

Figure 3: Hysteresis graph of the (a) magnitude characteristic and the (b) phase characteristic of the sample impedance.

It is highlighted that after several measurements it has been shown that, if certain techniques and circuitry are constructed, then the phase characteristic of GMI can be much more sensitive to magnetic fields than its counterpart magnitude characteristic [7,10].

Considering that, in the characterization studies, the impedance measurements of the GMI samples were performed by the LCR meter 4285A (Agilent), the uncertainties of the impedance magnitude, U_z, and phase, U_θ, measurements of the GMI samples are directly attributed to the uncertainties of the LCR meter, which are, respectively, defined in its operational manual as

$$U_z(\%) = \pm(A_n + A_c) \times K_t \text{ and} \qquad (7)$$

$$U_\theta(\text{degrees}) = \pm \frac{180 \times (A_n + A_c) \times K_t}{\pi \times 100}, \qquad (8)$$

where A_n is the component of the uncertainty due to the equipment intrinsic characteristics, A_c is the cable length factor and K_t is the temperature factor.

The temperature factor K_t is equal to one in the range of 18°C to 28°C. The measurements were always performed within this temperature range, then it can be admitted that $K_t = 1$.

Then, knowing that all of the experimental measurements of the impedance of the GMI sensors returned magnitude values between 10 mΩ and 100 Ω, the parameter A_n is defined as

$$A_n(\%) = N_2\% + \left(\frac{f_m}{30}\right)^2 \times 3\% + \frac{100}{|Z_m|}\left[0.02\% + \left(\frac{f_m}{30}\right) \times 0.1\%\right], \qquad (9)$$

where $|Z_m|$ is the absolute value of the measured impedance in ohms and N_2 is a frequency-dependent factor which can be equal to 0.15 – frequencies between 75 kHz and 3 MHz – or to 0.38 – frequencies above 3 MHz.

On the other hand, for impedance magnitudes below 5 kΩ, A_c is given by

$$A_c(\%) = \frac{f_m}{15}, \qquad (10)$$

where f_m is the frequency, in MHz, used to excite the sample.

The standard uncertainty of the magnetic field (u_H) generated by the Helmholtz pair is dependent of the standard uncertainty of the DC current source (Agilent, E3648A), which is equal to ±4.0 mA. Then, supposing, by simplicity, that the geometric configuration of the Helmholtz coils is satisfactorily close to the one considered on the theoretical model and knowing that the relation between the current and the magnetic field generated by the Helmholtz pair is given by (6), u_H is expressed as

$$u_H = \pm 228.97 \times u_I(A) = \pm 0.92\ Am^{-1}. \qquad (11)$$

Thus, the expanded uncertainty U_H, for a confidence level of 95.45%, is

$$U_H = 2 \times u_H = \pm 1.84\ Am^{-1}. \qquad (12)$$

The impedance measurement uncertainty U_z, of the results, obtained by applying equation (7) to the experimental data set, is always, at least, ten times smaller than its respective impedance value. All of the impedance phase values shown in this section have their respective measurement uncertainties U_θ, obtained by applying (8), equal or smaller than ± 1°.

The smallest magnetic field step used for the GMI samples characterization was 7.96 Am^{-1}, which is about 4

times larger than U_H (1.84 Am^{-1}). It is noticed that, in order to reduce the magnetic field step, it will be essential to improve the uncertainty of the current source.

4. RESULTS

The automated system has shown to be capable of acquiring a much larger amount of data than the manual process conventionally used [7] in the same timeframe.

An example of an automatic GMI sample characterization graph is depicted in Figure 4. The graph of the behavior of the inductive component of the GMI effect on the sample ribbon with the variation of the input current frequency is obtained by combining data from multiple automated experiments with the same measuring configurations, except for a single parameter – in this case the frequency of the excitation current). Each data series is consequently calculated by subtracting the origin inductance from every measurement. In this way, the result is related to the GMI equations (3) and (4). The clear tendencies of the inductive component observed in Figure 4 show the impact of the frequency on the GMI effect.

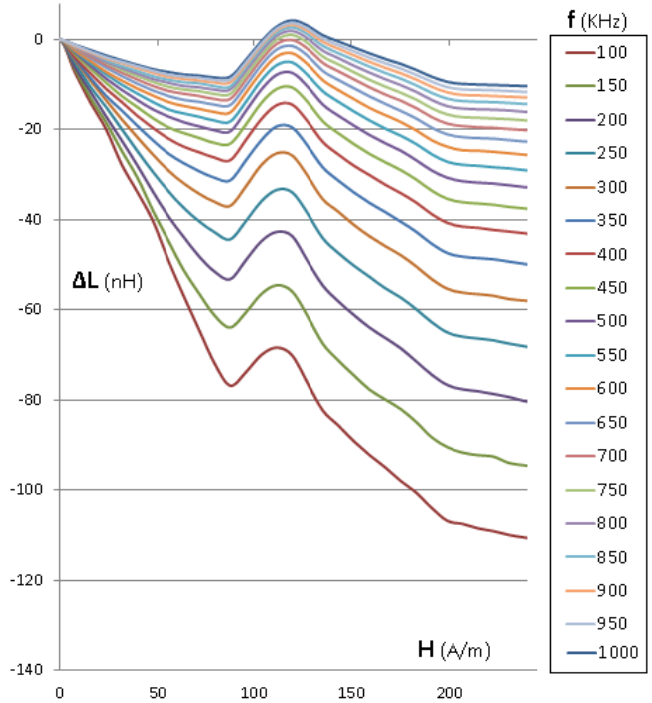

Figure 4: Inductance of a GMI sample of $Co_{70}Fe_5Si_{15}B_{10}$ alloy against external magnetic field. Each data series is obtained by varying the current frequency by 50 kHz, from 100 kHz to 1 MHz. The temperature (298 K) and the other electrical parameters (DC current = 80 mA; AC current = 15 mA) were kept constant.

These dependencies presented in Fig. 4 are also exhibited in the resistance, magnitude and phase characteristics and require a significant amount of data to be analyzed and consequently recognized, which demands long periods of time. For instance, to generate the data shown in Fig. 4 by means of a manual process, it would take approximately 19 hours of sequential experiments.

The software for automatic GMI sample characterization managed to generate all the tendencies of the inductive component of the GMI effect, presented in Fig. 4, plus the resistance component, $|Z|$ and θ characteristics in approximately 95 minutes. In other words, an experiment that would consume 1 hour using manual procedures takes 5 minutes using the current version of the automatic characterization system.

In this stage of research, the vast amount of data and variables that should be analyzed for optimizing the sensitivity of GMI sensor elements indicates the relevance of an automatic system for the characterization of GMI effect.

5. CONCLUSION

The developed system for automatic characterization of GMI samples, designed with the LabVIEW environment, allows the high speed identification of the impedance behavior as a function of specific measurement parameters. The attained performance is essential for the use of this tool to identify the optimal operational point of GMI magnetometers.

The number of external parameters controlled by the current system can be expanded, incorporating other aspects discussed in the literature [9], and this expansion is an objective of the LaBioMet team. Also, while the current version has shown a great improvement in speed for the characterization measurements, optimization in the LabVIEW code itself is being discussed in order to increase its performance even more.

Finally, the large amount of raw information requires some type of data filtering and analysis, since the tendencies identified by human eye recognition need to be captured by optimization algorithms.

In this way, a future version of the automatic characterization system would incorporate a feedback analysis to generate a new – and hopefully more insightful – list of experiment configurations, aiming at reaching an optimal point necessary for the development of a high sensitivity GMI magnetometer.

6. ACKNOWLEDGEMENTS

We thank the Brazilian funding agencies CNPq, FAPERJ and FINEP, for their financial support, and Prof. Fernando Machado (Dept. of Physics/UFPE) for the GMI samples provided.

7. REFERENCES

[1] A. E. Mahdi, L. Panina and D. Mapps, “Some new horizons in magnetic sensing: high-Tc SQUIDs, GMR and GMI materials,” Sensors and Actuators A: Physical, vol. 105, pp. 271-85, 2003.

[2] D. Robbes, C. Dolabdjian, S. Saez, Y. Monfort, G. Kaiser and P. Ciureanu, “Highly Sensitive Uncooled Magnetometers: State of the Art Superconducting Magnetic Hybrid Magnetometers, an alternative to SQUIDs?,” IEEE Transactions on Applied Superconductivity, vol. 2, no. 1, pp. 629-34, 2001.

[3] W. Andrä and H. Nowak, Magnetism in medicine: a handbook. 2nd Ed. Weinhein, Alemanha: WILEY-VCH, 2007.
[4] E. C. Silva, L. A. P. Gusmão, C. R. H. Barbosa, E. C. Monteiro and F. L. A. Machado, "Sensitivity improvement of GMI magnetic and pressure transducers for biomedical measurements," Braz. J. Biom. Eng., vol. 27, no. 2, pp. 1-11, 2011.
[5] D. R. Louzada, E. C. Monteiro, L. A. P. Gusmão, C. R. H. Barbosa, "Medição não-invasiva de ondas de pulso arterial utilizando transdutor de pressão MIG," in Proc. of IV Latin American Congress on Biomedical Engineering, IFMBE Proceedings, vol. 18, pp. 436-9, 2007.
[6] F. Pompéia, L. A. P. Gusmão, C. R. H. Barbosa, E. C. Monteiro, L. A. P. Gonçalves and F. L. A. Machado, "Ring shaped magnetic field transducer based on the GMI effect," Measurement Science and Technology, vol. 19 no. 2, 2008.
[7] E. C. Silva, L. A. P. Gusmão, C. R. H. Barbosa, E. C. Monteiro and F. L. A. Machado, "High sensitivity giant magneto-impedance (GMI) magnetic transducer: magnitude versus phase sensing," Measurement Science & Technology, vol. 22, no. 3, pp. 1-9, 2011.
[8] E. Costa Silva, L. A. P. Gusmão, C. R. Hall Barbosa and E. Costa Monteiro, "Progress Toward a Hundredfold Enhancement in the Impedance Phase Sensitivity of GMI Magnetic Sensors aiming at Biomagnetic Measurements," in Proc. of V Latin American Congress on Biomedical Engineering, IFMBE Proceedings, vol. 33, pp. 1-4, 2011.
[9] M. Phan and H. Peng, "Giant Magnetoimpedance materials: Fundamentals and applications," Progress in Materials Science, vol. 53, pp. 323-420, 2008.
[10] E. C. Silva, L. A. P. Gusmão, C. R. H. Barbosa and E. C. Monteiro, "Magnetic Field Transducers Based on the Phase Characteristics of GMI Sensors and Aimed at Biomedical Applications," in Proc. of 13th International Conference on Biomedical Engineering, vol. 23, pp. 652-56, 2009.
[11] K. C. Mendes and F. L. A. Machado, "Enhanced GMI in Ribbons of $Co_{70.4}Fe_{4.6}Si_{15}B_{10}$ Alloy," Journal of Magnetism and Magnetic Materials, vol. 177, pp. 111-12, 1998.
[12] K. C. Mendes and F. L. A. Machado, "Giant transversal magneto-impedance and Hall-effect measurements in $Co_{70.4}Fe_{4.6}Si_{15}B_{10}$," Journal of Applied Physics, vol. 79, no. 8, pp. 6555-8, 1996.